A Two-Dimensional Finite-Difference Solution for the Transient Thermal Behavior of a Tubular Solar Collector

F. L. Lansing
DSN Engineering Section

A numerical procedure was established using the finite-difference technique in the determination of the time-varying temperature distribution of a tubular solar collector under changing solar radiancy and ambient temperature. Three types of spatial discretization processes were considered and compared for their accuracy of computations and for selection of the shortest computer time and cost. The stability criteria of this technique was analyzed in detail to give the critical time increment to ensure stable computations. The results of the numerical analysis were in good agreement with the analytical solution previously reported. The numerical method proved to be a powerful tool in the investigation of the collector sensitivity to two different flow patterns and several flow control mechanisms.

I. Introduction

The need for an accurate prediction of the thermal behavior of solar collectors, to be used as a basic tool for their performance comparison, has become increasingly important with the rapid development of solar energy technology. For example, imposing changes on a specific solar collector such as introducing a new geometrical configuration, having a different control mechanism for its working fluid or developing new optical properties for the glazing and coating, require a sufficiently general analytical model which is both an adequate idealization of the physical system and capable of reasonably simple mathematical description.

The common procedure in analyzing the time-varying response of solar collectors has been based on a sequence of events of equal time intervals that range from 30 to 60 minutes, at the end of which the solar collector is assumed to have reached a quasi steady-state condition. This procedure cannot be generalized for all types of solar collectors and is restricted to those which possess very small thermal capacitance or very short response time (approximately 10 minutes) to the solar radiancy changes. The procedure would fit most flatplate collectors.

The solar collector under study has been selected as a candidate for Goldstone DSCC energy conservation pro-

jects. The time taken by this collector to reach quasi steady-state condition, measured experimentally by the solar simulator team at NASA Lewis Research Center, was approximately one hour. Accordingly, a new investigation was required for an accurate procedure to study its transient thermal behavior.

The possibility of finding an exact analytical solution was not excluded from the investigation and was reported in a previous article (Ref. 1). The first results indicated that the problem can be solved by a closed algebraic form, but it is highly complicated. To facilitate the computations, numerical solutions are preferred. The finite-difference method was then selected for the transient thermal study to supplement the analytical methods for additional coverage for this type of solar collector at all operating conditions.

II. Numerical Analysis

The numerical solution using the finite-difference method has become more popular in solving heat-transfer problems with the availability of high-speed digital computers and their associated technology. This method is used if a high degree of accuracy is required or if the problem is of considerable size and complexity.

In the finite-difference method, space and time discretization processes lead to a set of algebraic equations (nodal equations) instead of the partial differential equations that characterize the system. The nodal equations can be derived by purely mathematical methods or by energy consideration at the node of each spatial segment.

A. Collector Description and Flow Patterns

The tubular collector unit, as shown schematically in Figs. 1 and 2, is composed of three concentric tubes; an inner tube, an absorber tube, and a cover tube. The annulus space between the absorber and cover tubes is evacuated to minimize convection and conduction losses. The absorber tube surface is coated with a selective material to reduce the outward long-wave radiation losses. In flow pattern (1), as shown in Fig. 1 (a), the circulating fluid starts from the open-end section of the inner tube. At the closed end of the collector, the fluid reverses its direction and passes in the annulus spacing between the inner and absorber tubes. In flow pattern (2), as shown in Fig. 1 (b), the fluid path is reversed from the above. Each collector module consists of 24 collector units formed from flow patterns (1) and (2) in an alternate series as shown in Fig. 2. For more irradiancy augmentation, the set of collectors is mounted with lateral spaces separating them from each other with a highly reflective back reflector.

B. Program Procedure

Figure 3 illustrates one axisymmetric segment of the collector tube and the nodal and edge temperatures used throughout the analysis. The segment has a thickness ΔX and is bounded by sections (J) and $(J + 1)$ perpendicular to the axis of symmetry. The nodal temperatures of the Jth segment are located at the midsection of the segment and are denoted by TM_j. Four nodal temperatures are assigned to each segment, one for each of the following: the inner fluid pass, the outer fluid pass, the absorber tube surface, and the cover-tube surface temperatures. Because of the constrained boundary conditions at the open end and the closed end of each collector unit, as well as between the different flow patterns in series, the nodal temperatures of the fluid in the inner and outer passes only are converted back to the edge temperatures, after each computation process with an increment of time $\Delta\theta$. This results in a two-dimensional temperature distribution for the axisymmetric collector unit; in the axial direction and in the radial direction. No allowance is made for circumferential temperature differences between the upper tube's surface of the collector unit facing the Sun and the bottom tube's surface facing the back reflector. This means that the temperatures are uniform circumferentially.

The energy balance equations are listed in Appendix A for convenience. The present set of nodal and edge temperatures at time θ are then grouped together in a matrix format, and the corresponding future set of temperatures at time $(\theta + \Delta\theta)$ is then computed and updated using matrix multiplication algebra. The computations proceed in the above sequence after preassigning an initial set of temperatures. The latter can be arbitrarily determined based on past experience or can be given as a result of measurements.

III. Results and Conclusions

One of the obstacles that is met during the execution of the computations is the numerical instability. In Appendix B, the necessary stability criteria are derived and presented for each flow pattern. This shows that the increment time $\Delta\theta$ and the spatial increment ΔX cannot be arbitrarily chosen, but must be calculated from the above criteria to ensure stable computations. It can be shown from the critical stability condition Eq. (B-2), that

the smaller the size of each segment, ΔX, leads to a smaller allowable increment of time $\Delta\theta$ and a larger program execution time. This is due to the doubling of complexity; first due to the increased size of the matrices with larger number of segments, and second to the increased number of repetitions with smaller time intervals. Several program runs were made and the results are listed as follows:

(1) The time-varying temperature distribution of the working fluid in a unit collector at some given operating condition is plotted in Figs. 4 and 5 for flow patterns (1) and (2), respectively. The collector fluid temperature is assumed to be uniform at 70°C before a sudden step of solar radiancy of 0.75 kW/m^2 is imposed and remains constant thereafter. In both flow patterns, the steady-state exit fluid temperature reaches the same value of 78°C as shown in frame (d) of Figs. 4 and 5. It is clear from the time frames (a), (b) and (c) of Figs. 4 and 5, the distinct difference in responding to changes of the solar radiation between the different flow patterns. The exit fluid temperature of flow pattern (1) responds by a much faster rate in the early stages since the fluid leaves the collector as soon as it absorbs the useful energy from the annulus area facing the Sun. On the other hand, the exit fluid temperature of flow pattern (2) is not significantly increased until the relatively colder fluid in the center tube is discharged. This results in a much higher fluid temperature at the closed end of the collector which may cause some local degradations of the selective coating for this type of flow pattern.

(2) The exit fluid temperature obtained from the numerical results of the previous unit collector runs is plotted in Fig. 6. Superimposed on Fig. 6 is the analytical solution previously reported in Ref. (1) for the same operating conditions, optical and geometrical properties. Although the analytical solution was made with the assumption of zero tube thermal capacitance, it is in good agreement with the numerical solution which considers such a thermal capacitance with only a maximum deviation of $\pm$ 0.5°C. The deviation between the numerical and analytical solutions in the first 5 min in Fig. 6 is due to the different estimates of the initial temperature profile. The analytical solution considers an initial steady-state temperature profile with inlet fluid temperature of 70°C, which results in an exit temperature of 69.2°C, (Ref. 1), while the numerical solution arbitrarily assigns a uniform fluid temperature of 70°C in the two fluid passes.

(3) The finite-difference numerical solution is then applied to two collector units connected in series as shown in Fig. 2. In this case, the following two important criteria have been studied:

(a) The effect of changing the diameter of the inner tube on the rate of temperature growth is plotted as shown in Fig. 7. The manufacturer's specification of the inner diameter, D_i, is 10.5 mm, which makes the fluid velocity in the inner fluid pass seventeen times larger than the fluid velocity in the annulus pass. The reason for that selection is to shorten the residence time inside the center tube for faster extraction of the hot fluid, though it causes an excessive impulse force at the closed-end of the collector. On the other hand, the minimization of these impulsive forces requires that the velocity in each fluid pass should be equal and the inner diameter in this case would be 29 mm. It is clear from Fig. 7 that reducing the diameter D_i will hasten the response of the collector after about 20 min, though it has no effect on the steady-state temperature that could be reached.

(b) The rate of cooling of the collector at zero solar radiation is illustrated in Fig. 8. The fluid in the two collector units is assumed uniform at 87°C when a sudden drop of the solar radiation to zero value is imposed and remains constant thereafter. The rate of cooling amounts to 2.9°C/h to an ambient temperature of 30°C. This shows the very low heat loss coefficient that this collector possesses over flat plate types. This is mainly due to the vacuum employed and the use of selective coatings.

(4) The application of the numerical solution has been extended further to study a complete module, consisting of 24 collector units connected in series with alternating flow patterns. Three different computer programs have been written corresponding to three different space discretization processes for $N = 4$, 2 and 1. This results in a substantial reduction of computer time and cost as the number of segments per tube is reduced. For example, the computer time is approximately in the ratio of 16:4:1 as the number of segments N goes from 4:2:1, respectively. This is due to the squared-reduction effects of matrices size and the number of time loops required. Regarding accuracy, it has been found that increasing the space segments has an insignificant effect as shown in Fig. 9. The temperature deviation is shown to be $\pm$ 1 percent as the number of segments N is reduced from 2 to 1 which was done to obtain a 75 percent reduction of the computer time and cost.

(5) The practical use of the tubular solar collector has indicated that the maximum end-to-end temperature rise across one module can reach as high as 50°C or approxi-

mately 2°C for each collector unit. This low temperature differential of the working fluid results in an insignificant temperature gradient across both the cover and absorber tube ends. Several module runs with three types of spatial divisions (four, two and one-segment per tube) indicate that the one-segment solution is more than adequate for the temperature profile prediction without sacrificing accuracy. The four-segment solution is not recommended as it consumes excessive computer time (at least 16 times that of a one-segment solution). The two-segment solution may or may not be used for further studies, depending on the allowable program funds.

(6) The collector circulating fluid may be stopped during operation at the following two time periods as a temperature vs. flow control technique: (a) from midnight to about 8:00 a.m. when the sun starts to rise, and (b) from the sunset at about 7:00 p.m. to midnight. The control system is designed to conserve what is collected during the sunshine hours. The actual hours of operation vary from day to day, depending on the type of application and the solar radiation time.

To allow for this, the numerical analysis program is provided with two extra computational controls. The first handles the periods of shut-down when all the 24 collector units behave as a single collector unit regardless of flow patterns, as occurs when the module end-to-end temperature difference is zero or 2°C at the maximum. The second computational control deals with sudden diurnal shut down after operation with a module end-to-end temperature difference exceeding 2°C.

(7) In Fig. 10 the results of six different flow control processes are plotted for a collector module (24 units in series) under variable solar radiancy and ambient temperatures. The total incident solar radiation falling on a plane surface at 20°C with the horizontal and facing south is registered and plotted for June 2, 1975 at the Goldstone DSCC, California. The accumulated solar irradiancy for that day was 10.465 kWh/m^2 and with a collector module projected area of 2.602 m^2, the total incident energy amounted to 27.228 kWh. The numerical analysis provided a valuable assistance in exposing the transient thermal behavior of the collector under several flow controls and the understanding of its important features. The flow control processes are as follows:

(a) *Flow Control* (1): The fluid is left stagnant starting at midnight with a temperature of 20°C equal to the ambient temperature. During the sunshine period, the temperature rises and reaches a maximum of 230°C at around 4:00 a.m. under the given solar radiancy. The slow rate of cooling as discussed in item (3) b, will keep the fluid hot most of the time, and the temperature will reach about 130°C at the following midnight. Since no drainage of hot water is assumed in this control, the overall thermal collection efficiency will be zero.

(b) *Flow Control* (2): This is similar to flow control (1) except that the fluid is left stagnant starting midnight at a temperature of 70°C. At about 6:00 a.m. the fluid temperature drops by 13°C due to night cooling, and then starts to pick up some heat as the sun rises. The maximum temperature is found to be 244°C at 4:00 p.m. and it drops to 130°C at the following midnight as in flow control (1). The overall thermal collection efficiency is also zero with this control. The results from flow controls (1) and (2) indicate that the no-flow maximum fluid temperature, though not significantly varying with the temperature of the residing fluid at midnight, can reach excessive values that cause severe thermal stresses and coating degradation problems.

(c) *Flow Control* (3): This is a modification of flow control (1) whereby the fluid is left stagnant starting midnight with 20°C temperature and after reaching a temperature of 70°C at about 9 a.m., a fluid circulating pump is turned on and a uniform flow rate of 22 kg/h from the storage tank flows into the collector. The fluid temperature oscillates around 130°C for 5½ hours (10:30 a.m. to 4:00 p.m.) and then drops to 70°C at about 7:00 p.m. The peak of the accumulated thermal energy for the day occurs at 7:00 p.m. and reaches 36.23 percent of the total incident solar energy.

(d) *Flow Control* (4): This is the same as flow control (3) except that the pump is rated at 33 kg/h. The fluid temperature thus oscillates about 110°C for 5½ h (10:30 a.m. to 4:00 p.m.); a temperature and a range most suitable for running an absorption type of air conditioner. The peak of the accumulated thermal energy for the day occurs at 6:30 p.m. and reaches 37.39 percent of the total incident solar energy.

(e) *Flow Control* (5): This is a modification of flow control (2) whereby the fluid is left stagnant starting midnight with 70°C temperature and after reaching a temperature of 70°C at 8:00 a.m., a fluid circulating pump is turned on and a uniform flow rate of 33 kg/h from the storage tank flows into the collector. The fluid temperature oscillates around 110°C for about 7 h (9:15 a.m. to 4:00 p.m.) which is longer than the range given by flow control (4). The peak of the accumulated thermal

energy for the day occurs at 6:30 p.m. and reaches 42.34 percent of the total incident solar energy.

(f) *Flow Control* (6): This is a continuous pumping operation for 24 h with a flow rate of 33 kg/h of the fluid at 70°C starting at midnight. The temperature drop for the period from midnight to 5:00 a.m. is only 5°C. As the Sun rises, the fluid temperature starts to increase and matches the temperatures reached by flow controls (4) and (5). The peak of the accumulated thermal energy occurs at 6:30 p.m. and reaches 41.72 percent of the total incident solar energy.

It is clear from the above six trials of flow control that flow control (5) provides the highest accumulated thermal efficiency (42.34%) as well as the required hot temperature (110°C) for an airconditioning application over a period of about 7 h (9:15 a.m. to 4:00 p.m.).

Definition of Terms

C Specific heat of tube material, kWh/kg • °C

C_f Specific heat of flowing fluid, kWh/kg • °C

D Tube diameter, m

F Augmented radiation factor, ≥ 1

G_{mn} Thermal conductance, kW/m²

I Direct solar radiancy, kW/m²

L Tube length, m

m_f Fluid mass flow rate, kg/h

N Number of space elements per tube,

Q_{in} Nodal internal heat generation, kWh

r Reflectivity,

T Edge temperature, K

TM Nodal temperature, K

T_{sky} Sky temperature, K

T_{amb} Ambient temperature, K

U_{ac} Radiative heat transfer coefficient between the absorber and the cover tubes, kW/m² • °C

U_{ao} Overall heat transfer coefficient between the absorber tube and the outer fluid in the annulus, kW/m² • °C

U_{cv} Convective heat transfer coefficient between the cover tube and the ambient air, kW/m² • °C

U_{oi} Overall heat transfer coefficient between the outer fluid and the inner fluid, kW/m² • °C

U_{rd} Radiative heat transfer coefficient between the cover tube and sky, kW/m² • °C

V Volume, m³

X Distance measured from the inlet tube section, m

θ Time, h

α Absorptivity

ϵ Emissivity

τ Transmissivity of cover tube

δ Tube thickness, m

ρ Density, kg/m³

Δ Increment

Subscripts

$_a$ absorber tube

$_c$ cover tube

$_f$ fluid

$_i$ inner fluid, in the center tube

$_o$ outer fluid, in the annulus area

Acknowledgement

The author would like to acknowledge Dr. C. L. Hamilton who provided valuable assistance in the technical analysis and R. J. Wallace and K. P. Bartos who made a number of helpful suggestions.

References

1. Lansing, F. L., "The Transient Thermal Response of a Tubular Solar Collector," *Technical Memorandum 33-781*, Jet Propulsion Laboratory, Pasadena, Calif., July 15, 1976.
2. Razelos, P., "Methods of Obtaining Approximate Solutions," *Handbook of Heat Transfer*, edited by Rohsenow, W. M., and Hartnett, J. P., Sec. 4, McGraw Hill Book Co., N. Y., 1973.

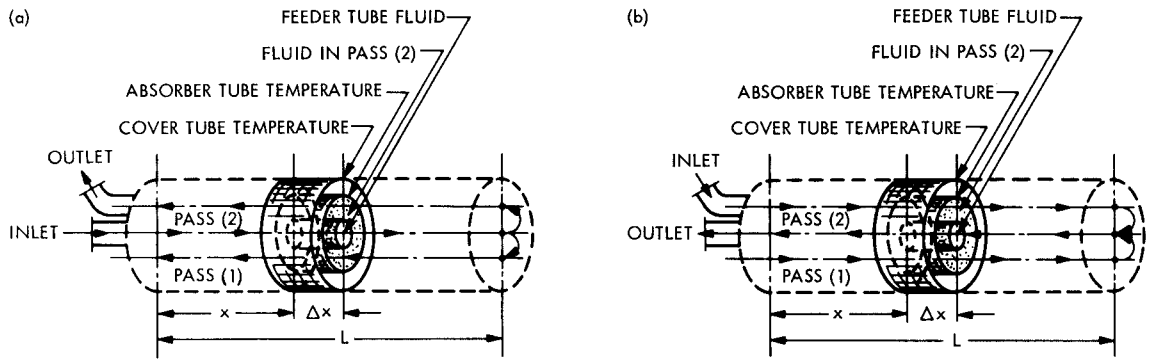

Fig. 1. Collector configuration (a) flow pattern (1) (b) flow pattern (2)

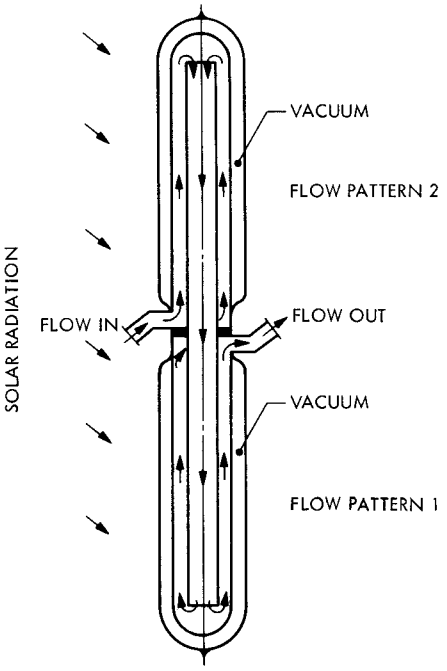

Fig. 2. Two collector units in series

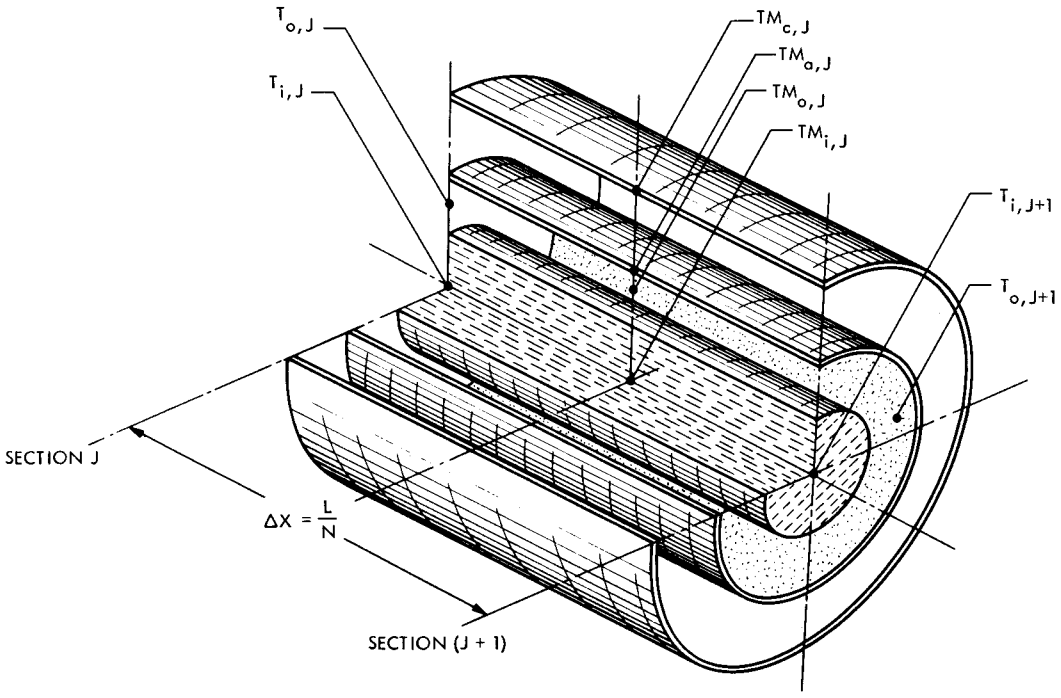

Fig. 3. Nodal and edge temperatures of the Jth segment

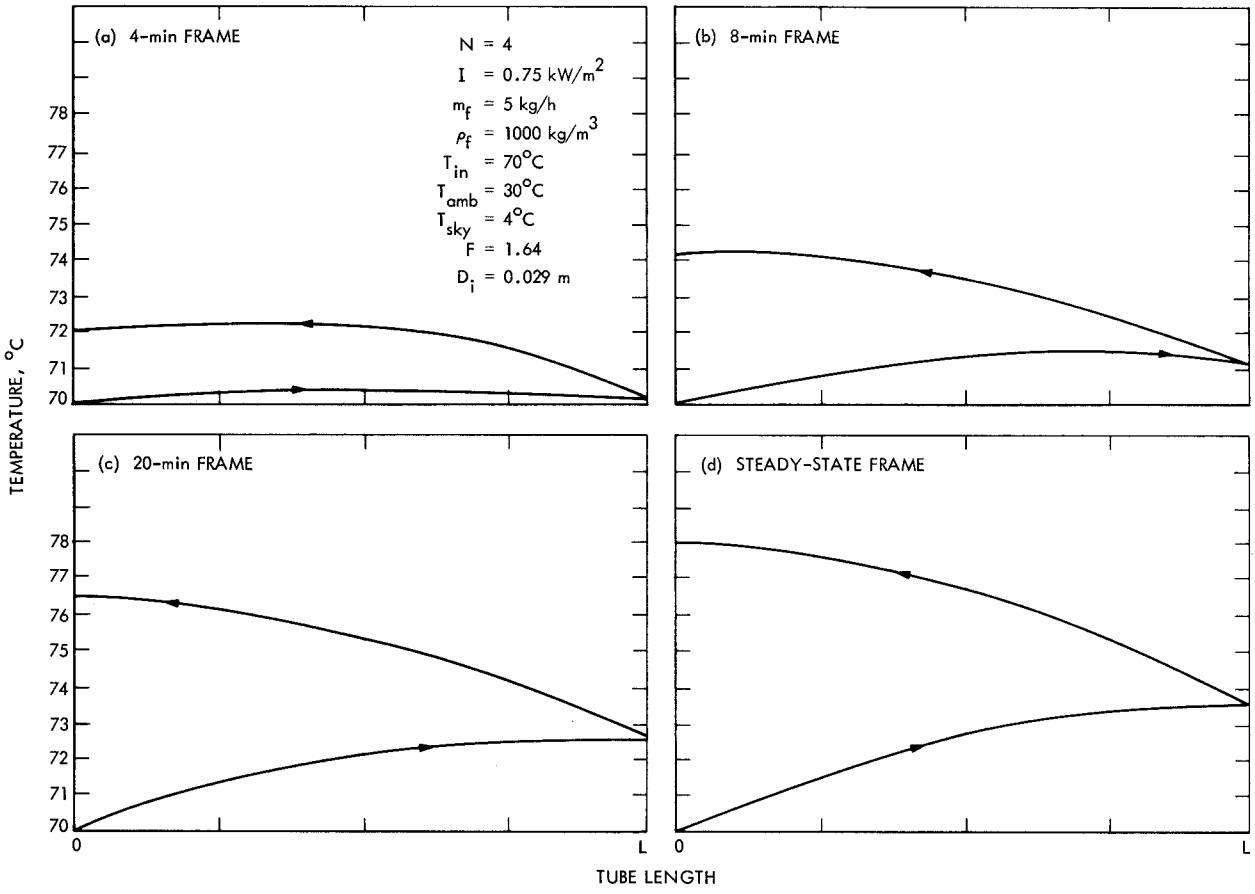

Fig. 4. Different time frames for one collector unit of flow pattern (1) showing the growth of the temperature profile

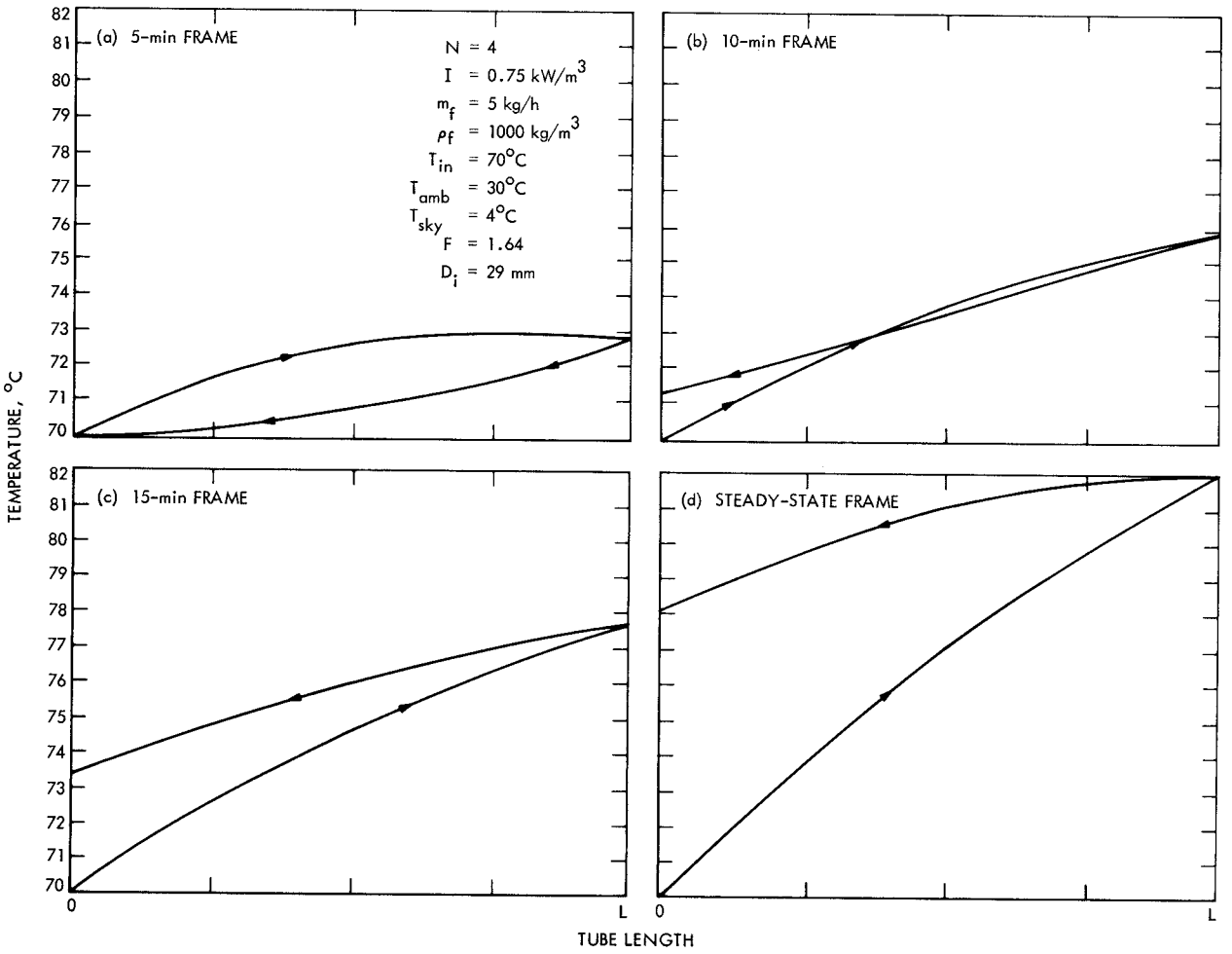

Fig. 5. Different time frames for one collector unit of flow pattern (2) showing the growth of the temperature profile

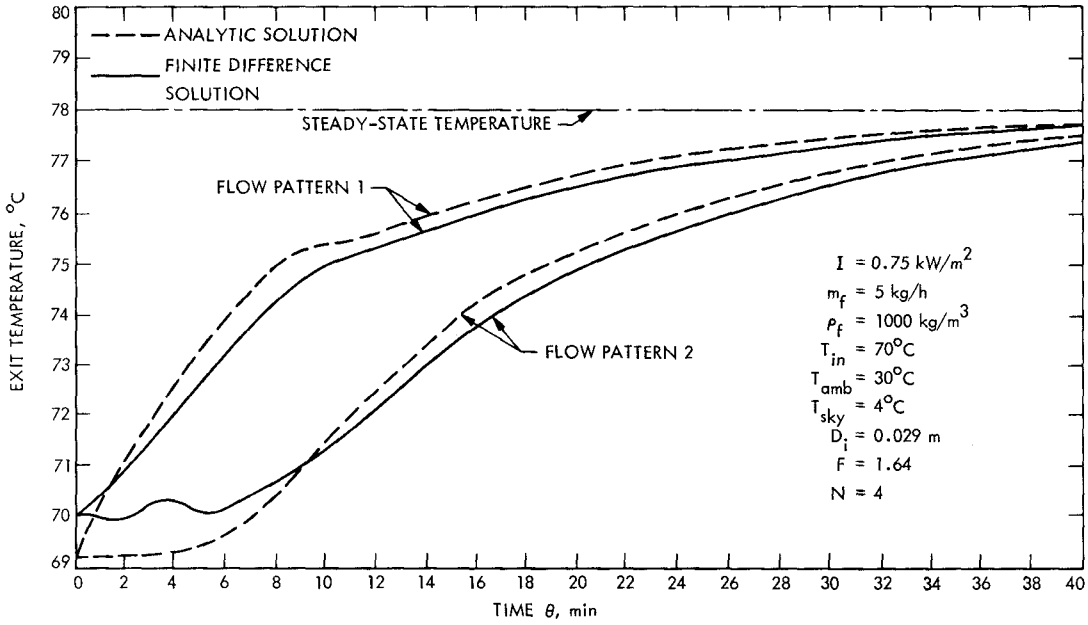

Fig. 6. Comparison between the finite difference solution and the analytical solution for a single tube and two different flow patterns

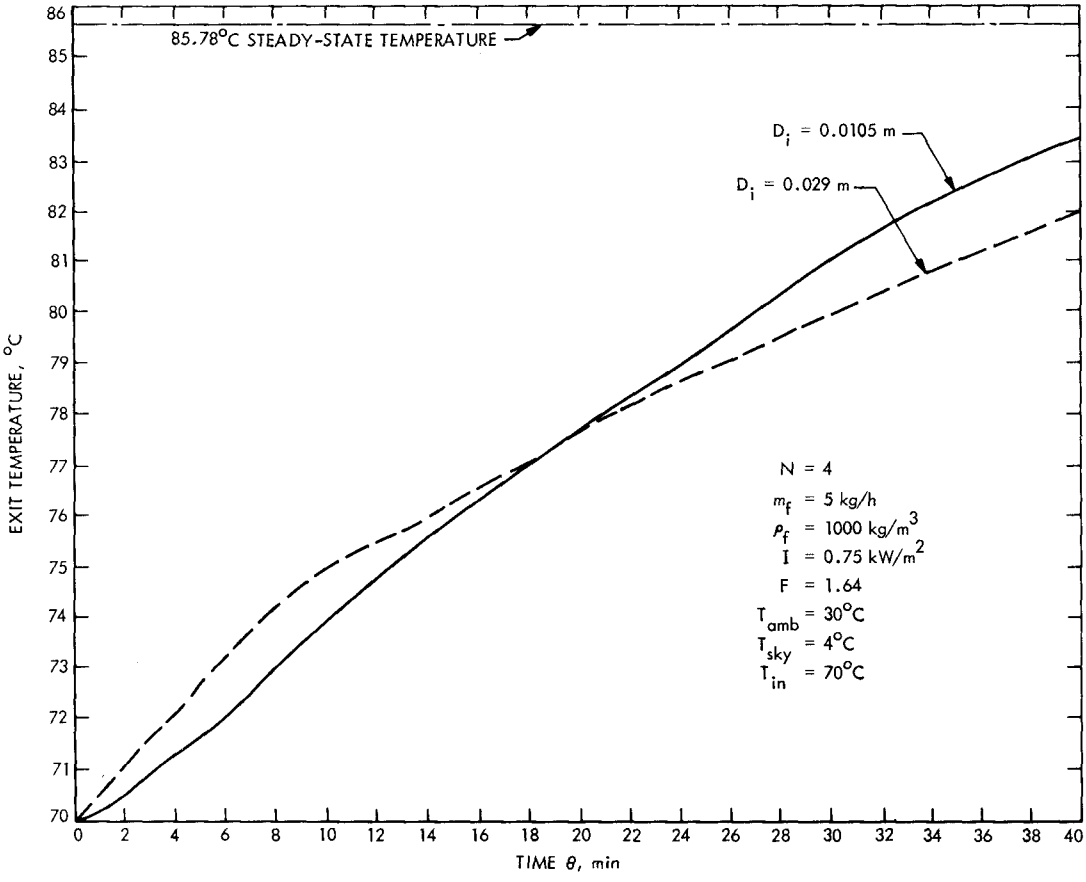

Fig. 7. Effect of increasing the inner tube diameter on thermal response for two collector units in series

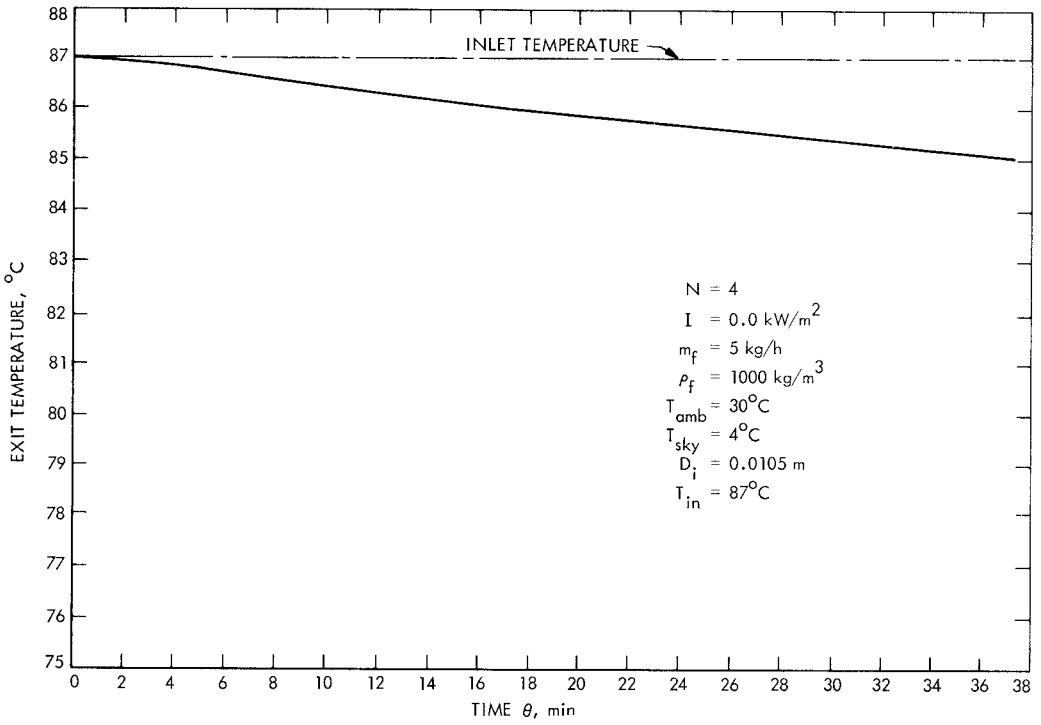

Fig. 8. Rate of cooling of two collector units in series at zero radiancy and constant inlet fluid temperature

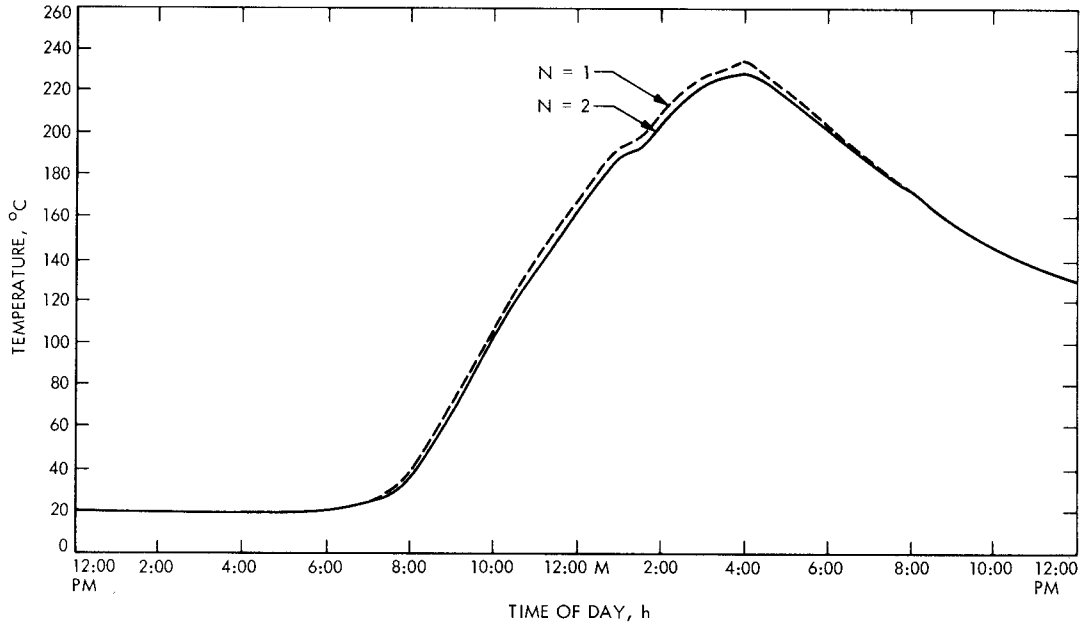

Fig. 9. Temperature deviations as calculated numerically for two finite-difference schemes with different space segments for 24 collector units at zero flowrate

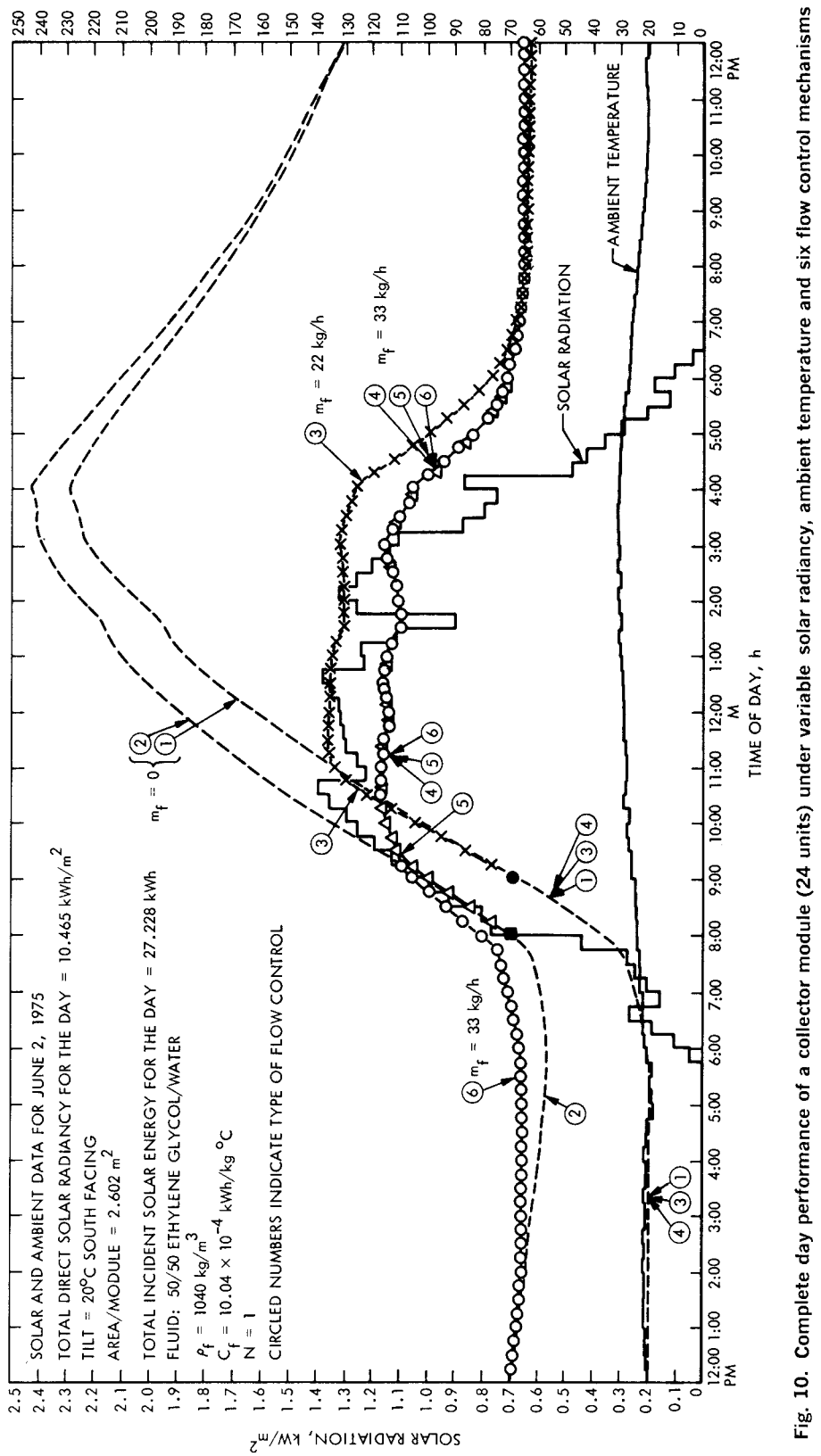

Fig. 10. Complete day performance of a collector module (24 units) under variable solar radiancy, ambient temperature and six flow control mechanisms

Appendix A

Nodal Energy Equations

I. General Remarks

The first step in obtaining the nodal equations is to subdivide the collector tubes into spatial segments by sections as shown in Fig. 3, locate a node in the center of each segment and then calculate the conductances between adjacent nodes. The energy balance for the mth node which is surrounded by n adjacent nodes, is then considered during a small time interval $\Delta\theta$. During this time interval, the temperatures of the n nodes are assumed to remain constant. Accordingly,

$$\rho_m C_m V_m \frac{\Delta T_m}{\Delta\theta} = \sum_n G_{mn} [T_n(\theta) - T_m(\theta)] + Q_{in} \tag{A-1}$$

where V_m is the volume assigned to the segment whose node is m, G_{mn} is the thermal conductance between nodes m, n, and Q_{in} is the rate of heat generation in the node if any. The difference ΔT_m may be expressed in terms of either a forward, a backward or a mid-difference (Ref. 2) which will yield different forms of Eq. (A-1). The simplest form is obtained using the "forward" difference and is chosen for the present work, i.e.,

$$\Delta T_m = T_m(\theta + \Delta\theta) - T_m(\theta) \tag{A-2}$$

In this case, the future temperature $T_m(\theta + \Delta\theta)$ is explicitly obtained from the knowledge of the present temperatures $T_m(\theta)$ and $T_n(\theta)$ at time θ. Combining Eqs. (A-1) and(A-2) gives the future temperature $T_m(\theta + \Delta\theta)$ as follows:

$$T_m(\theta + \Delta\theta) = T_m(\theta) + \left[\sum_n G_{mn} [T_n(\theta) - T_m(\theta)] + Q_{in}\right] \frac{\Delta\theta}{\rho_m C_m V_m} \tag{A-3}$$

It is important to note that the conductances G_{mn} include, in general, the energy conducted across the tube boundaries of the elements as well as the energy transported between neighboring nodes in case of an open system node with a fluid flowing across the segment (Lagrangian control volume approach).

II. Boundary Conditions

(1) For both flow patterns the closed-end temperature of the inner and the outer fluid must be equal.

(2) For flow pattern (1), the open-end temperature of the fluid in the inner tube is a known value.

(3) For flow pattern (2), the open-end temperature of the fluid in the annulus area is a known value.

(4) For a collector composed of two tubes of flow pattern (1) and (2) in series, the open end-to-end temperatures must be equal.

III. Energy Equations

The application of Eq. (A-3) ot the inner fluid, outer fluid, absorber tube and the cover tube segments yield the following:[1]

A. Inner Fluid

$$TM_{i,j}(\theta + \Delta\theta) = TM_{i,j}(\theta) + \left[G_{oi} [TM_{o,j}(\theta) - TM_{i,j}(\theta)] \pm G_{ff} [T_{i,j+1}(\theta) - T_{i,j}(\theta)]\right] \frac{\Delta\theta}{\rho_f C_f \frac{V_i}{N}} \tag{A-4}$$

where the (+) sign is for flow pattern (2) and the (−) sign is for flow pattern (1).

Expressing the inner fluid nodal temperatures in terms of the edge temperatures as

$$TM_{i,j}(\theta) = \frac{T_{i,j}(\theta) + T_{i,j+1}(\theta)}{2}$$
$$TM_{o,j}(\theta) = \frac{T_{o,j}(\theta) + T_{o,j+1}(\theta)}{2} \tag{A-5}$$

Then

$$\begin{aligned} TM_{i,j}(\theta + \Delta\theta) = {} & T_{i,j}(\theta)[0.5 - (0.5\, G_{oi}\Delta\theta_i \pm G_{ff}\Delta\theta_i)] \\ & + T_{i,j+1}(\theta)[0.5 - 0.5\, G_{oi}\Delta\theta_i \pm G_{ff}\Delta\theta_i] \\ & + T_{o,j}(\theta)\{0.5\, G_{oi}\Delta\theta_i\} \\ & + T_{o,j+1}(\theta)\{0.5\, G_{oi}\Delta\theta_i\} \end{aligned} \tag{A-6}$$

[1]See Appendix A of Ref. (1) for the explanation and the derivation of the heat flux distribution.

where

$$G_{oi} = U_{oi}\frac{\pi D_i L}{N}$$

$$G_{ff} = m_f C_f$$

$$V_i = \frac{\pi}{4} D_i^2 L$$

$$\Delta\theta_i = \frac{\Delta\theta \cdot N}{\rho_f C_f \cdot \frac{\pi}{4} D_i^2 L} \tag{A-7}$$

and the (+) sign is for flow pattern (2) and the (−) sign is for flow pattern (1).

B. Outer Fluid

$$TM_{o,j}(\theta + \Delta\theta) = TM_{o,j}(\theta) + \left[\left(U_{ao}\frac{\pi D_a L}{N}\right)[TM_{a,j}(\theta) - TM_{o,j}(\theta)] - \left(U_{oi}\frac{\pi D_i L}{N}\right)[TM_{o,j}(\theta) - TM_{i,j}(\theta)] \mp (m_f C_f)[T_{o,j+1}(\theta) - T_{o,j}(\theta)]\right] \cdot \frac{\Delta\theta}{\rho_f C_f \frac{V_o}{N}} \tag{A-8}$$

where the (+) sign is for flow pattern (1) and the (−) sign for flow pattern (2).

Expressing the outer fluid nodal temperatures in terms of edge temperatures as

$$TM_{o,j}(\theta) = \frac{TM_{o,j}(\theta) + TM_{o,j+1}(\theta)}{2}$$

$$TM_{i,j}(\theta) = \frac{TM_{i,j}(\theta) + TM_{i,j-1}(\theta)}{2} \tag{A-9}$$

Then

$$\begin{aligned} TM_{o,j}(\theta + \Delta\theta) = {} & T_{o,j}(\theta)\{0.5 - (0.5\,G_{ao}\Delta\theta_o \\ & + 0.5\,G_{oi}\Delta\theta_o \mp G_{ff}\Delta\theta_o)\} \\ & + T_{o,j+1}(\theta)\{0.5 - 0.5\,G_{ao}\Delta\theta_o \\ & - 0.5\,G_{oi}\Delta\theta_o \mp G_{ff}\Delta\theta_o\} \\ & + TM_{a,j}(\theta)\{G_{ao} \cdot \Delta\theta_o\} \\ & + T_{i,j}(\theta)\{0.5\,G_{oi}\Delta\theta_o\} \\ & + T_{i,j+1}(\theta)\{0.5\,G_{oi}\Delta\theta_o\} \end{aligned} \tag{A-10}$$

where

$$G_{ao} = U_{ao} \cdot \frac{\pi D_a L}{N}$$

$$G_{oi} = U_{oi}\frac{\pi D_i L}{N}$$

$$G_{ff} = m_f C_f$$

$$V_o = \frac{\pi}{4}(D_a^2 - D_i^2)L$$

$$\Delta\theta_o = \frac{\Delta\theta \cdot N}{\rho_f C_f (D_a^2 - D_i^2)L} \tag{A-11}$$

and the (+) sign is for flow pattern (1) and the (−) sign is for flow pattern (2).

C. Absorber Tube

$$TM_{a,j}(\theta + \Delta\theta) = TM_{a,j}(\theta) + \left[I \cdot F \cdot \left(\frac{\alpha_a \tau_c}{1 - r_a r_c}\right) \cdot \frac{D_c L}{N} - \left(U_{ao}\frac{\pi D_a L}{N}\right)[TM_{a,j}(\theta) - TM_{o,j}(\theta)] - \left(U_{ac}\frac{\pi D_a L}{N}\right)[TM_{a,j}(\theta) - TM_{c,j}(\theta)]\right] \times \frac{\Delta\theta}{\rho_a C_a \frac{V_a}{N}} \tag{A-12}$$

Expressing the outer fluid nodal temperatures in terms of edge temperatures as

$$TM_{o,j}(\theta) = \frac{T_{o,j}(\theta) + T_{o,j+1}(\theta)}{2} \tag{A-13}$$

Hence

$$\begin{aligned} TM_{a,j}(\theta + \Delta\theta) = {} & TM_{a,j}(\theta)\{1 - G_{ao}\Delta\theta_a - G_{ac}\Delta\theta_a\} \\ & + TM_{c,j}(\theta)\{G_{ac}\Delta\theta_a\} \\ & + T_{o,j}(\theta)\{0.5\,G_{ao}\Delta\theta_a\} \\ & + T_{o,j+1}(\theta)\{0.5\,G_{ao}\Delta\theta_a\} \\ & + \left\{I \cdot F \cdot \frac{\alpha_a \tau_c}{1 - r_a r_c} \cdot \frac{D_c L}{N} \cdot \Delta\theta_a\right\} \end{aligned} \tag{A-14}$$

where

$$V_a = \pi D_a \delta_a L$$

$$\Delta\theta_a = \frac{\Delta\theta \cdot N}{\rho_a C_a \cdot (\pi D_a \delta_a L)} \tag{A-15}$$

D. Cover Tube

$$TM_{c,j}(\theta + \Delta\theta) = TM_{c,j}(\theta) + \left\{\left\{I \cdot F \cdot \left(\alpha_c + \frac{\alpha_c r_a r_c}{1 - r_a r_c}\right) \cdot \frac{D_c L}{N}\right\} + U_{ac}\frac{\pi D_a L}{N}[TM_{a,j}(\theta) - TM_{c,j}(\theta)] - U_{cr} \cdot \frac{\pi D_c L}{N}[TM_{c,j}(\theta) - T_{\text{amb}}] - U_{rd} \cdot \frac{\pi D_c L}{N}[TM_{c,j}(\theta) - T_{\text{sky}}]\right\} \frac{\Delta\theta}{\rho_c C_c \frac{V_c}{N}} \tag{A-16}$$

or

$$TM_{c,j}(\theta+\Delta\theta) = TM_{c,j}(\theta)[1 - G_{ac} \cdot \Delta\theta_c - G_{cb}\Delta\theta_c - G_{cs}\Delta\theta_c] + TM_{a,j}(\theta)[G_{ac} \cdot \Delta\theta_c] + \Delta\theta_c \left\{\left\{I \cdot F \cdot \left(\alpha_c + \frac{\alpha_c r_a \tau_a}{1 - r_a r_c}\right)\frac{D_c L}{N}\right\} + (G_{cb} \cdot T_{amb}) + (G_{cs} \cdot T_{sky})\right\} \tag{A-17}$$

where

$$V_c = \pi D_c \delta_c L$$

$$\Delta\theta_c = \frac{\Delta\theta \cdot N}{\rho_c C_c (\pi D_c \delta_c L)}$$

$$G_{cb} = U_{cr}\frac{\pi D_c L}{N}$$

$$G_{cs} = \frac{U_{rd} \cdot \pi D_c L}{N} \tag{A-18}$$

Appendix B

Convergence and Stability of Computations

I. General Remarks

In the numerical computations, the term error refers to the difference between the approximate solution obtained by the finite difference scheme and the exact solution of the original partial differential equations. Accordingly, there exists two types of errors.

(1) Truncation error due to the replacement of the derivatives by finite differences. This depends on the given initial and boundary conditions.

(2) Round-off error caused by carrying out the computations to a finite decimal place.

Apart from the above errors, the most serious problem associated with the finite difference scheme is the phenomena of instability. This means that the temperatures oscillate with an increasing magnitude as the computation progresses. Therefore, the space and time increments ΔX, $\Delta\theta$, respectively, cannot be selected arbitrarily but rather constrained to satisfy certain stability criteria. For practical applications, the following elementary argument (Ref. 2) has been used for obtaining simple and adequate stability conditions.

The mth node temperature can be expressed in terms of the surrounding n nodes in the format:

$$T_m(\theta + \Delta\theta) = K_{mm}T_m(\theta) + \sum_n K_{mn}T_n(\theta) \qquad \text{(B-1)}$$

where the coefficients K_{mn} are set to be positive. If the coefficient K_{mm} was negative then the higher temperature $T_m(\theta)$ at the present time θ, the lower the temperature $T_m(\theta + \Delta\theta)$ at the future time $(\theta + \Delta\theta)$. This would be in violation of the thermodynamics principles. Therefore, the increment of time $\Delta\theta$ for a given space subdivision ΔX should be chosen so that the coefficient K_{mm} is positive or at least zero. Applying the above simple rule to the finite difference equations developed earlier for each node, the following critical stability conditions are established.

II. Case of Flow Pattern (1)

For the inner fluid temperature stability

$$0.5 - 0.5\,G_{oi}\Delta\theta_i - G_{ff}\Delta\theta_i \geq 0 \qquad \text{(B-2)}$$

For the outer fluid temperature stability

$$0.5 - 0.5\,G_{ao}\Delta\theta_o - 0.5\,G_{oi}\Delta\theta_o - G_{ff}\Delta\theta_o - 0.5\,G_{oi}\Delta\theta_i \geq 0 \qquad \text{(B-3)}$$

For the absorber tube temperature stability

$$1 - (G_{ao} + G_{ac})\,\Delta\theta_a \geq 0 \qquad \text{(B-4)}$$

For the cover tube temperature stability

$$1 - (G_{ac} + G_{cb} + G_{cs})\,\Delta\theta_c \geq 0 \qquad \text{(B-5)}$$

III. Case of Flow Pattern (2)

For the inner fluid temperature stability

$$0.5 - G_{ff}\Delta\theta_i - 0.5\,G_{oi}\Delta\theta_i - 0.5\,G_{oi}\Delta\theta_o \geq 0 \qquad \text{(B-6)}$$

For the outer fluid temperature stability

$$0.5 - 0.5\,G_{ao}\Delta\theta_o - 0.5\,G_{oi}\Delta\theta_o - G_{ff}\Delta\theta_o \geq 0 \qquad \text{(B-7)}$$

For the absorber tube temperature stability

$$1 - (G_{ao} + G_{ac})\,\Delta\theta_a \geq 0 \qquad \text{(B-8)}$$

For the cover tube temperature stability

$$1 - (G_{ac} + G_{cb} + G_{cs})\,\Delta\theta_c \geq 0 \qquad \text{(B-9)}$$

IV. Case of a Series Connection of Flow Patterns (1) and (2)

The foregoing conditions are combined and listed as follows:

For the inner fluid temperatures stability, a comparison of conditions (B-2) and (B-3) shows that condition (B-4) predominates, thus leaving

$$0.5 - G_{ff}\Delta\theta_i - 0.5\,G_{oi}\Delta\theta_i - 0.5\,G_{oi}\Delta\theta_o \geq 0$$

or

$$\Delta\theta \leq \frac{\rho_f C_f}{(4U_{oi}/D_i) + (8N\,C_f m_f/\pi D_i^2 L) + \left[4U_{oi}/(D_o^2/D_i)\left(1 - \left(\frac{D_i}{D_a}\right)^2\right)\right]} \tag{B-10}$$

For the outer fluid temperature stability, a comparison of conditions (B-3) and (B-7) shows that condition (B-7) predominates, thus

$$0.5 - 0.5\,G_{ao}\Delta\theta_o - 0.5\,G_{oi}\Delta\theta_o - G_{ff}\Delta\theta_o - 0.5\,G_{oi}\Delta\theta_i \geq 0$$

or

$$\Delta\theta \leq \frac{\rho_f C_f}{\left(\frac{4U_{oi}}{D_i}\right) + \frac{8N\,m_f C_f}{\pi(D_a^2 - D_i^2)L} + \frac{4U_{oi}}{D_a \cdot \left(\frac{D_a}{D_i}\right) \cdot \left(1 - \left(\frac{D_i}{D_a}\right)^2\right)} + \frac{4U_{ao}}{D_a\left[1 - \left(\frac{D_i}{D_a}\right)^2\right]}} \tag{B-11}$$

For the absorber tube temperatures stability

$$1 - (G_{ao} + G_{ac})\,\Delta\theta_a \geq 0$$

or

$$\Delta\theta \leq \frac{\rho_a C_a \delta_a}{(U_{ao} + U_{ac})} \tag{B-12}$$

For the cover tube temperature stability

$$1 - (G_{ac} + G_{cb} + G_{cs})\,\Delta\theta_c \geq 0$$

or

$$\Delta\theta \leq \frac{\rho_c C_c \delta_c}{\left(U_{ac}\frac{D_a}{D_c} + U_{cv} + U_{rd}\right)} \tag{B-13}$$

V. Example of Computations for the Critical Time Increment

To determine which of the above four conditions, Eqs. (B-10), (B-11), (B-12) and (B-13) yield the most critical time increment $\Delta\theta$ to ensure stable temperature computations, the following numerical values are assigned from a typical running condition:

$D_i = 0.0105$ m, $\quad \delta_a = \delta_c = 0.004$ m

$D_a = 0.041$ m, $\quad C_f = 11.634 \times 10^{-4}$ kWh/Kg · °C (water)

$D_c = 0.051$ m, $\quad C_c = C_a = 2.094 \times 10^{-4}$ kWh/Kg · °C (glass)

$L = 1.067$ m, $\quad \rho_f = 1000$ kg/m³ (water)

$N = 4$ $\quad \rho_c = \rho_a = 2468$ kg/m³ (glass)

$m_f = 5$ kg/h

$U_{oi} = 56.53 \times 10^{-3}$ kW/m² · °C

$U_{ao} = 113.06 \times 10^{-3}$ kW/m² · °C

$U_{ac} = 0.80 \times 10^{-3}$ kW/m² · °C

$U_{cv} = 18.62 \times 10^{-3}$ kW/m² · °C

$U_{rd} = 4.99 \times 10^{-3}$ kW/m² · °C

Condition (B-10) yields $\Delta\theta \leq 0.0022$ h (7.8 s)

Condition (B-11) yields $\Delta\theta \leq 0.0166$ h (59.7 s)

Condition (B-12) yields $\Delta\theta \leq 0.0182$ h (65.4 s)

Condition (B-13) yields $\Delta\theta \leq 0.0852$ h (306.7 s)

The above indicates that Condition (B-10) is the most critical condition that must be satisfied in order to ensure stable computations. It can be seen from Condition (B-10) that the resulting minimum increment of time is inversely proportional with the mass flowrate. In the limit, with zero fluid flowrate, Condition (B-10) yields $\Delta\theta \leq 0.0505$ h (181.8 s) and in this case Condition (B-12) will impose the minimum time required for stable computations.

With regard to accuracy, the round-off errors have little or no effect on the solution if the restrictions of stability are observed, while the truncation errors decrease as we select smaller time and space increments.